


μ POP Clock: A Microcell Atomic Clock Based on a Double-Resonance Ramsey Scheme

Etienne Batori^{1,*}, Christoph Affolderbach¹, Matthieu Pellaton¹, Florian Gruet¹, Maddalena Violetti^{2,3}, Yuanyan Su², Anja K. Skrivervik² and Gaetano Mileti¹

¹University of Neuchâtel, Institute of Physics, Laboratoire Temps-Fréquence, Avenue de Bellevaux 51, 2000 Neuchâtel, Switzerland

²École Polytechnique Fédérale de Lausanne, Microwave and Antenna Group (MAG), SCI-STI-AS, Station 11, 1015 Lausanne, Switzerland

³Fondazione Toscana Life Sciences, Via Fiorentina 1, 53100 Siena, Italy

 (Received 4 April 2022; revised 2 September 2022; accepted 26 September 2022; published 14 November 2022)

We demonstrate and study a microcell microwave atomic clock based on optical-microwave double resonance (DR) interrogation operated in a pulsed Ramsey scheme, called the μ POP clock, based on a microfabricated Rb vapor cell and a micro-loop-gap microwave resonator. For the mm-scale dimensions of this cell, the population and coherence relaxation rates of the Rb clock transition are on the order of 4–5 kHz, which puts constraints on the useful Ramsey times and overall pulse sequence in view of optimized clock performance. Our proof-of-principle demonstration of the μ POP clock shows that the pulsed DR approach is nevertheless feasible and results in a short-term clock stability of $1 \times 10^{-11} \tau^{-1/2}$ and reaching the $\leq 2 \times 10^{-12}$ level at timescales of 1000 s to one day. The short-term instability budget established for the μ POP clock shows that the main limitation to the short-term stability arises from the detection noise. Thanks to the pulsed Ramsey scheme, light-shift effects are strongly reduced in the μ POP clock, which opens perspectives for further improvements of long-term clock stability, in view of future generations of miniature vapor-cell clocks with enhanced performances based on the DR scheme.

DOI: 10.1103/PhysRevApplied.18.054039

I. INTRODUCTION

Since their initial laboratory demonstration roughly 20 years ago, miniature or “chip-scale atomic clocks” (CSACs) [1,2] have retained a high level of interest and research activities. Key performance specifications of such CSAC realizations are a small volume ($< 15 \text{ mm}^3$), low power consumption ($< 120 \text{ mW}$), and a frequency instability of few $10^{-10} \tau^{-1/2}$ and around 1×10^{-11} at one day. With this, CSACs are of high interest for applications in telecommunication networks [3], remote or distributed sensor arrays, such as for ocean bottom seismology [4], and for improved Global Navigation Satellite Systems (GNSS) receivers [5].

Such CSACs exploit the ground-state microwave reference transition in alkali atoms contained in a microfabricated vapor cell [6]. This reference can conveniently be detected using coherent population trapping spectroscopy (CPT) [7] using a vertical-cavity surface-emitting laser (VCSEL) directly modulated at the microwave transition frequency [8]. The CPT approach allows extreme miniaturization and low power consumption, but also comes with drawbacks of small signal contrasts (1% level) and is particularly sensitive to light-shift effects [9,10] that limit the long-term stability, which is one of the key specifications of interest for an atomic clock.

Pulsed CPT interrogation in the Ramsey scheme [11,12] allows for narrower linewidth and reduced light-shift effects, as studied on cm-scale hot atomic vapor cells [13–17] and laser-cooled atomic samples [18]. Recently, pulsed CPT schemes were also studied for application to microfabricated vapor cells and clocks demonstrating short-term clock stabilities around 4 to 9×10^{-11} at one second. The medium-term clock stability reached 4×10^{-12} at 10^4 s , constituting a factor of 20 improvement

*etienne.batori@unine.ch

Published by the American Physical Society under the terms of the Creative Commons Attribution 4.0 International license. Further distribution of this work must maintain attribution to the author(s) and the published article's title, journal citation, and DOI.

compared to the same clock in cw operation, corresponding to similarly reduced light-shift effects [14,19].

In contrast to CPT, the “classical” optical-microwave double-resonance (DR) clock approach [20] uses direct coupling of the microwave radiation to the atomic sample, and has some distinct advantages. Notably, Ramsey-mode DR-based clocks using cm-scale vapor cells achieve signal contrasts of $C=20\text{--}30\%$ or more, resulting in excellent short-term clock stabilities of few $10^{-13} \tau^{-1/2}$ and state-of-the-art long-term stabilities on the level of 1×10^{-14} or better at one day [21–24], with small instability contributions from light-shift effects [25,26]. It was quantified that in these Ramsey-mode DR clocks the long-term instability contribution due to light-shift effects is reduced by at least one order of magnitude or more, compared to an optimized cw DR clock [27]. It may thus be expected that applying the Ramsey DR scheme to miniature atomic clocks can overcome the present limitations in such clocks, including CPT-based CSAC, towards long-term stabilities on the level of 10^{-12} or better at timescales of one day and beyond.

Early studies on a cw DR microcell atomic clock with a short-term stability of $2 \times 10^{-11} \tau^{-1/2}$ were reported in Ref. [28] and demonstrated the competitiveness of this approach. However, the possible advantages of Ramsey-mode operation of a DR microcell clock have not been studied yet.

In the present work, we investigate the μ POP clock, using a Ramsey-mode DR scheme applied to a micro-fabricated vapor cell. This scheme allows for a strong suppression of light-shift effects compared to cw operation and bears high potential for improved long-term clock stability to the 10^{-12} level at a few hours to one day timescales, thus outperforming current CSAC long-term stability.

II. EXPERIMENTAL APPROACH

In ^{87}Rb atomic clocks, the $\nu_0 \approx 6.8347\text{-GHz}$ ground-state microwave transition $5S_{1/2}, |F=1, m_F=0\rangle \leftrightarrow |F=2, m_F=0\rangle$ serves as stable atomic reference [see Fig. 1(a)]. The microwave transition is enhanced and detected using a light field, such as the 780.24-nm D2-line transition, coupling one of the ground states to an excited state [20]. In the pulsed Ramsey-mode DR scheme (also referred to as POP clock) we apply a series of distinct interrogation steps to the atomic sample held in the microcell, separated in time [see Fig. 1(b)]. First, a strong optical pump pulse (duration t_p) accumulates the atomic ground-state population into one single state. Then, two microwave $\pi/2$ pulses (duration t_m), separated by a Ramsey time T_R , drive the atomic ground-state transition. Finally, the atomic transition probability is read out with a weak optical detection pulse (duration t_d) and the signal is constituted by the absorption of the detection pulse by the

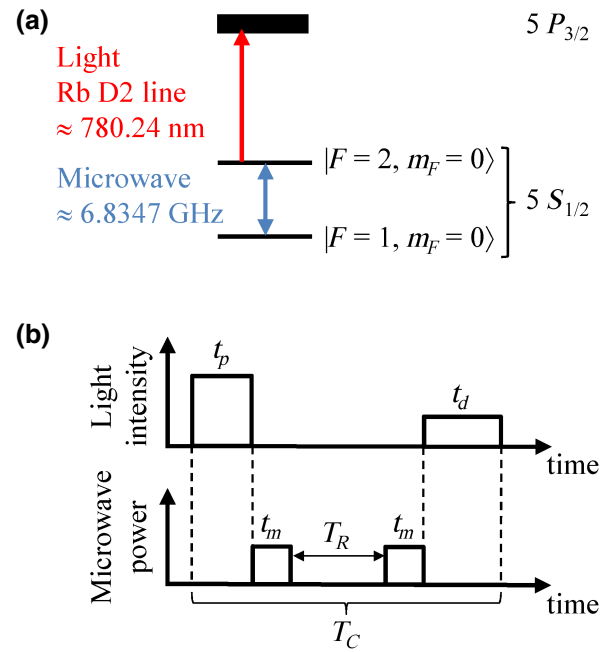


FIG. 1. (a) Rb level scheme. (b) Optical and microwave pulse sequence for the Ramsey scheme.

atomic vapor, detected on a photodetector placed behind the cell.

The experimental setup used in this study is schematically presented in Fig. 2 and described in more detail in the following sections. The microfabricated Rb cell is placed in a miniature microwave resonator, the micro-loop-gap resonator (μ LGR) [29], see Sec. II A. Light pulses are generated by a custom-made stabilized laser head, see Sec. II B. The microwave signal is provided by a low-noise microwave synthesizer, piloted by a state machine that also controls the clock PI loop.

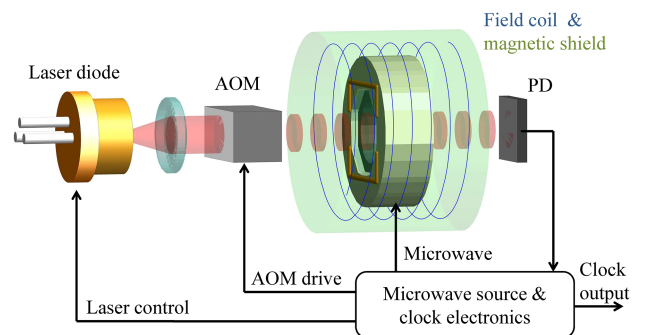


FIG. 2. Schematics of the μ POP clock setup. The microcell is held inside the μ LGR resonator, the whole surrounded by field coils and a magnetic shield. 780-nm light from a laser diode is switched using an acousto-optical modulator (AOM). A photodetector (PD) detects the optical signal.

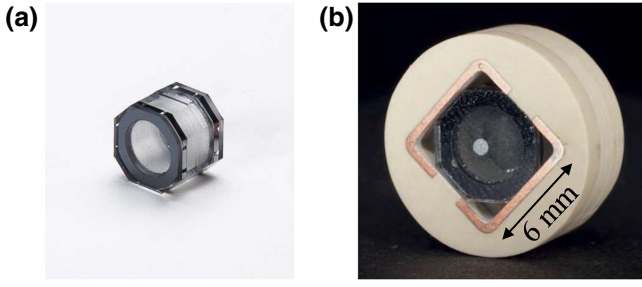


FIG. 3. Photographs of (a) the Rb microcell, and (b) the μLGR microwave resonator holding the cell. The external diameter of the white dielectric is 11 mm.

A. Microcell and atomic resonator

The microcell used [30] is fabricated from silicon and glass wafers using anodic bonding techniques and has an internal size of 4 mm diameter and 4.1 mm height [see Fig. 3(a)]. It contains Rb atomic vapor in natural isotopic mixture and an Ar-N₂ buffer-gas mixture ($P_{Ar}/P_{N_2} = 1.27$, 55 mbar total pressure). The cell temperature is 99 °C for a density of 2.5×10^{10} atoms/mm³ [31]. The cell is held inside the μLGR miniature microwave resonator [29] used to apply the microwave radiation to the atomic sample. The μLGR [see Fig. 3(b)] consists of four layers of square-shaped metallic electrodes, patterned on three layers of dielectric substrates using printed-circuit-board techniques [29], which makes this type of microwave resonator suitable for miniature atomic clock realizations. The μLGR shows a small volume of <0.9 cm³ and a high field orientation factor [32] that favors selective interrogation of the desired microwave clock transition. It has a moderate Q factor of approximately equal to 100 and a coupling of $S_{11} = -15$ dB on resonance.

B. Laser source

For this proof-of-concept study, the optical pump and detection pulses are generated by a custom-made frequency-stabilized laser head also integrating an acousto-optical modulator as the fast optical switch [33, 34]. The laser emits at 780.24 nm, resonant with the ⁸⁷Rb D2-line transition from $5S_{1/2}, F = 1$ ground-state level to the $5P_{3/2}$ multiplet. Maximum output power is around 7 mW, in a 0.78 mm² cross-section beam ($1/e^2$ area). Typical relative intensity and relative frequency stabilities [35] are presented on Table I. A typical detection relative intensity noise (RIN) spectrum is presented on Fig. 4. The RIN is measured after the vapor cell to account for noise conversion in the atomic vapor [36].

C. Microwave source

The clock electronics unit, similar to the one described in Ref. [37], handles the pattern generation (transistor-transistor logic pulses for laser switching) and generation

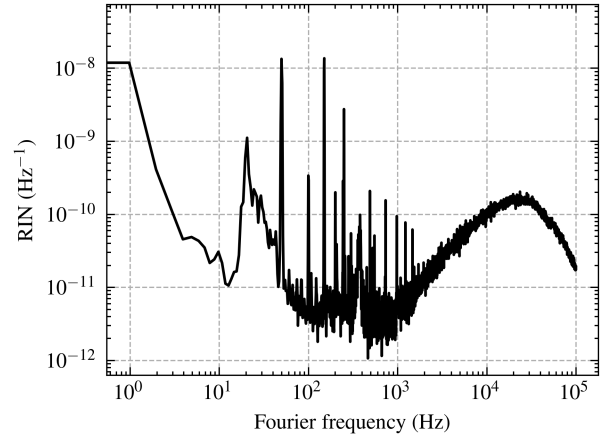


FIG. 4. Typical spectrum of detection noise in terms of RIN, measured after the vapor cell.

of the 6.834 GHz ⁸⁷Rb clock transition microwave frequency, by up-conversion from a 10-MHz quartz oscillator. The microwave pulses have sufficiently low phase noise (< -110 dBc/Hz from $T_C^{-1} \approx 1$ kHz) to minimize the Dick effect, see Sec. III C.

III. RESULTS

A. Ramsey fringes

Typical Ramsey fringes of the μPOP clock in nominal conditions are presented on Fig. 5. The chosen time steps of the sequence are $t_p = 200 \mu s$, $t_m = 46 \mu s$, $T_R = 290 \mu s$, and $t_d = 200 \mu s$, resulting in a total cycle time $T_C = 2t_m + t_d + t_p + T_R = 782 \mu s$. The microwave power is adjusted to +1.3 dBm to achieve short $\pi/2$ pulses. The contrast is 6.7% (peak-to-peak amplitude of the central fringe divided by the central fringe maximum) and the FWHM is 1.43 kHz, in agreement with the well-known relation for the Q -factor [38]:

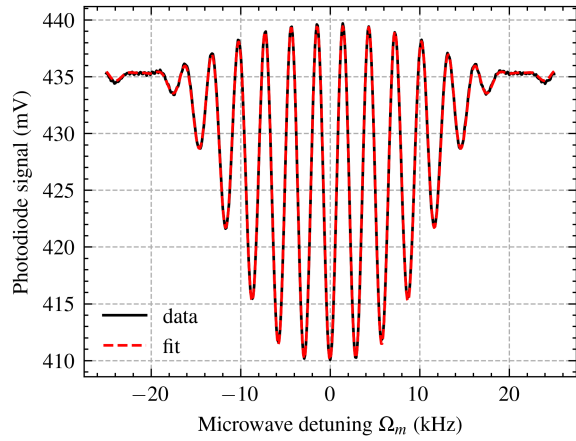
$$Q = \frac{\nu_0}{\text{FWHM}} = 2\nu_0 \left(T_R + \frac{4}{\pi} t_m \right). \quad (1)$$

B. Relaxation rates

The achievable fringe widths at useful signal contrast and thus the achievable short-term stability are physically limited by the population and coherence relaxation rates, γ_1 and γ_2 , respectively, of the Rb ground-state transition in

TABLE I. Typical laser head intensity and frequency relative stabilities, in pulsed operation.

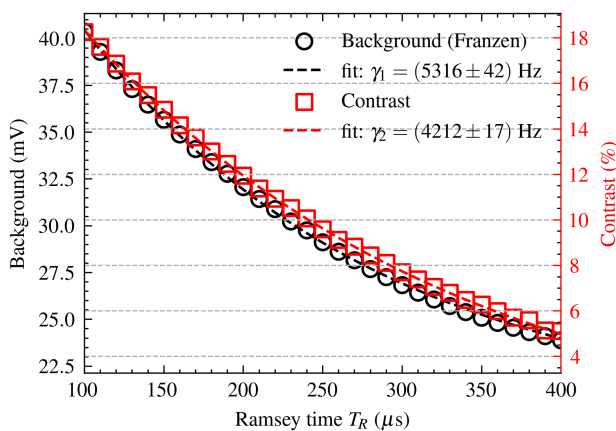
	1 s	10 ⁴ s
Rel. intensity stability	2×10^{-2}	3×10^{-3}
Rel. frequency stability	3×10^{-11}	3×10^{-10}


 FIG. 5. Typical Ramsey fringes of the μ POP clock.

our mm-scale microcell. Indeed, the signal amplitude, contrast, and background decrease exponentially with increasing Ramsey and microwave times, T_R and t_m . In particular, for fixed t_m [39],

$$C \propto e^{-\gamma_2 T_R}, \quad (2)$$

which is used to fit γ_2 that impacts on the signal contrast and thus the obtainable clock stability. γ_1 is measured using the signal background via the Franzen method [40] and mainly impacts on the signal background and the fringe envelope [41,42]. Numerical fits to the experimental data shown in Fig. 6 yield $\gamma_1 \approx 5.3$ kHz and $\gamma_2 \approx 4.2$ kHz, corresponding to relaxation times $T_i = \gamma_i^{-1}$ of $T_1 \approx 190$ μ s and $T_2 \approx 240$ μ s, respectively, thus restricting the useful Ramsey times to $T_R \lesssim 250$ μ s. For comparison, this is approximately 10 times shorter than the $T_R \approx 3$ ms typically used in high-performance cell clocks based on glass-blown cells of, e.g., 25 mm diameter and length showing $T_1 = 3.2$ ms and $T_2 = 4.3$ ms [43].


 FIG. 6. Exponential dependence of fringe contrast and transmitted signal as a function of Ramsey time T_R .

C. Signal optimization

One possible and simple metric for optimization of the clock's parameters is maximizing the product of contrast and quality factor, the CQ factor [19,44]. For this purpose, Ramsey fringes are acquired for Ramsey times T_R varying from 100 to 450 μ s, to measure the corresponding C and Q . The result of this CQ optimization is shown in Fig. 7 and yields an optimal T_R of 180 μ s.

However, this CQ optimization consists of an approximative optimization of the SNR. Indeed, because of the pulsed operation, the sampling of the optical detection noise into the clock's short-term stability must be considered.

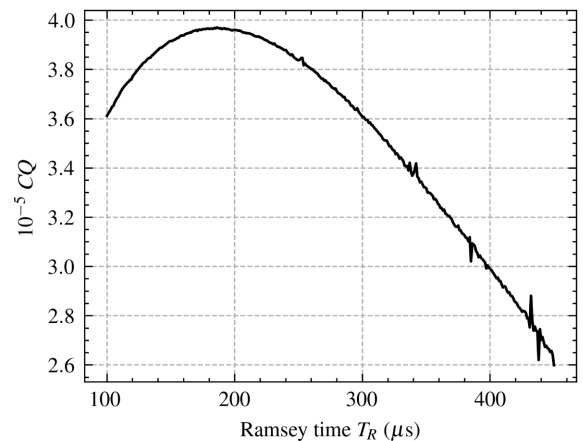
In the following, we analyze simultaneously the SNR and Dick-effect contributions for the μ POP clock to directly minimize its short-term stability given by

$$\sigma_y^{\text{total}}(\tau) = \sqrt{\sigma_y^{\text{SNR}}(\tau)^2 + \sigma_y^{\text{Dick}}(\tau)^2}. \quad (3)$$

The SNR contribution reads [45]

$$\sigma_y^{\text{SNR}}(\tau) = \frac{2(1 - C/2)}{\pi CQ} \times \left(\sum_{\substack{k > 0 \\ k \text{ odd}}}^{\infty} \text{sinc}^2 \left(\frac{k\pi t_d}{2T_C} \right) S_{\text{RIN}} \left(\frac{k}{2T_C} \right) \right)^{1/2} \tau^{-1/2} \quad (4)$$

with C the contrast, S_{RIN} the one-sided detection's RIN and Q the signal's quality factor from Eq. (1).


 FIG. 7. CQ as a function of T_R , determined from a series of 350 Ramsey signals, yielding an optimal $T_R \approx 180$ μ s.

The Dick effect contribution reads [46]

$$\sigma_y^{\text{Dick}}(\tau) = \left(\sum_{k=1}^{\infty} \text{sinc}^2 \left(\frac{k\pi T_R}{T_C} \right) S_y^{\text{LO}} \left(\frac{k}{T_C} \right) \right)^{1/2} \tau^{-1/2}, \quad (5)$$

with S_y^{LO} the local-oscillator frequency noise spectrum measured at nominal output power.

The optimization of Eq. (3) is a trade-off. Maximizing the detection and Ramsey duty cycles, respectively, $d_d = t_d/T_C$ and $d_R = T_R/T_C$ tends to minimize the infinite sums in Eqs. (4) and (5) but at the price of lower contrast and lower photodiode signal, which increases the prefactor in Eq. (4) and increases the RIN, thus degrading the clock stability. For instance, t_p and consequently T_C can be reduced in order to increase the duty cycles, as long as the contrast is not diminished. For the same reason, the microwave time t_m is set to the lowest possible value (which is limited by the maximum microwave power) for realizing $\pi/2$ pulses. Optimization of T_R is similar, with the difference that long T_R also improve the quality factor, Eq. (1) leading to a different trade-off.

Full optimization of T_R around the nominal other parameters is shown on Fig. 8. For each T_R , Eqs. (4) and (5) are computed with the other cycle's durations fixed to the optimal ones presented in Sec. III A and using the measured C and Q data from Fig. 7. From 0 to 150 μs , the Dick-effect contribution is dominant and decreases with increasing Ramsey time, whereas the SNR limit becomes dominant from 150 μs . It increases as the contrast and relevant RIN decrease with increasing T_R . The optimal Ramsey time region is wide and rather shallow and goes from 150 to 300 μs . For our study we set $T_R = 290 \mu\text{s}$ because it experimentally shows the best short-term stability and gives an

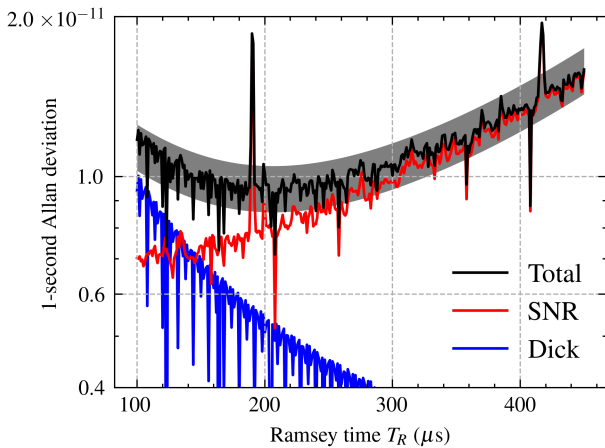


FIG. 8. Estimated SNR contribution, Dick-effect contribution and total limit to the short-term stability, as a function of T_R . The gray region represents the 10% experimental uncertainty in the estimation of the total short-term stability.

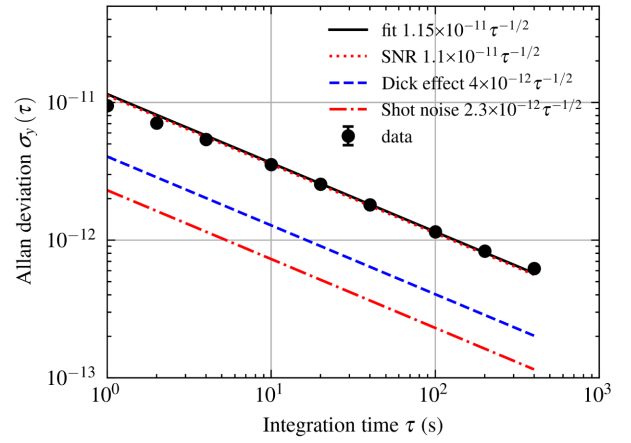


FIG. 9. Clock's short-term stability. The behavior of the stability from 1 to 5 s slightly deviates from the expected $\tau^{-1/2}$ power law because of a low integrator loop gain.

additional margin on the Dick-effect contribution. Note that in the case of μ POP, the SNR contribution as a function of T_R is most sensitive to the variation of d_d and RIN degradation, which explains why the CQ optimum at $T_R = 180 \mu\text{s}$ seen on Fig. 7 is barely noticeable on Fig. 8. The final, optimized pulse durations are those given in Sec. III A.

IV. CLOCK STABILITY

For clock measurements, the microwave frequency applied to the μ LGR is stabilized to the center of the observed fringes (see Fig. 5) using frequency modulation by half the fringe width (approximately equal to ± 700 Hz) and subsequent lock-in detection to stabilize the 10-MHz frequency of the quartz oscillator. The quartz output frequency is then compared to an in-house H-maser reference [47].

A. Short-term stability

The measured short-term stability (see Fig. 9 and Table II) is $1.15 \times 10^{-11} \tau^{-1/2}$ and is dominated by the SNR contribution, with a small contribution of the Dick effect. Preliminary estimations show that the light-shift contributions are negligible contributors of the short-term stability, at least 2 orders of magnitude below the measured stability.

B. Long-term stability and performance enhancement

Figure 10 shows the long-term stability of the μ POP clock, compared to the one for cw operation of the same clock setup, as well as to other microcell and miniature microwave atomic clocks. At short timescales, the μ POP clock stability is roughly 2 times better than in cw operation and at least 5 times to 1 order of magnitude better than its competitors. For comparison, the contrast and FWHM

TABLE II. Short-term stability budget. The intensity and frequency light-shift contributions are consistent with white noise up to 50 s [35].

Contribution	$\sigma_y(\tau)$
SNR (theory)	$1.1 \times 10^{-11} \tau^{-1/2}$
<i>of which shot-noise limit</i>	$2.3 \times 10^{-12} \tau^{-1/2}$
Dick effect (theory)	$0.4 \times 10^{-11} \tau^{-1/2}$
Intensity light shift (measured)	$1.8 \times 10^{-13} \tau^{-1/2}$
Frequency light shift (measured)	$9.1 \times 10^{-16} \tau^{-1/2}$
Total (theory)	$1.2 \times 10^{-11} \tau^{-1/2}$
Measured	$1.15 \times 10^{-11} \tau^{-1/2}$

of the cw version are 15% and 10 kHz, respectively, resulting in a roughly 3 times worse CQ factor compared to the μ POP. From 10^3 s integration time and beyond, the performances of the μ POP clock is improved by 1 order of magnitude compared to the cw case, reaching 5×10^{-13} at 2000 s and 2×10^{-12} at 2×10^5 s. This result establishes the current state of the art for a microcell microwave atomic clock. We further note that the μ POP clock performance of 5×10^{-13} at $\tau = 2000$ s comes very close to the stability of 3×10^{-13} at these timescales reported in Ref. [48] for a microcell optical atomic clock using a much more complex optical clock architecture.

From the measured light-shift coefficients and laser characteristics [33] we estimate the long-term instability contribution from the frequency and intensity light shifts to be of the order of 2.45×10^{-14} and 2.47×10^{-13} , respectively, at least one order of magnitude below the measured stability.

The strong reduction of the light-shift effects opens perspectives for further improvements on the long-term stability of the μ POP clock, provided the other now dominating limitations can be understood and controlled. A detailed full metrological study of the long-term stability budget has been initiated and is currently on going.

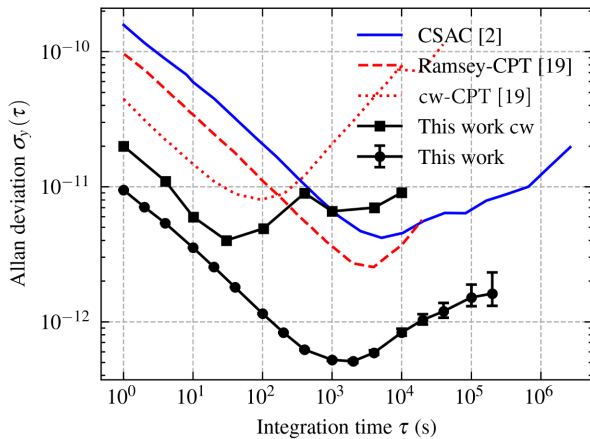


FIG. 10. Allan deviation of the μ POP clock, compared to other microcell atomic clocks.

V. CONCLUSIONS

We report a proof-of-principle study of the DR μ POP clock, in view of reducing light-shift effects for improved long-term stability of microcell microwave atomic clocks. The short-term stability is 1.15×10^{-11} at one second and in good agreement with the instability budget. The long-term stability is below 1×10^{-12} from 200 s to 10^4 s and $\leq 2 \times 10^{-12}$ at 2 days. Thanks to the POP scheme, the light-shift effect is strongly reduced and the medium- to long-term performances are consequently up to 1 order of magnitude better than in cw operation of the same physics' package and outperform other CPT-based microcell clocks. In pulsed mode, we observe an improvement of the short-term stability compared to cw mode, which is not reported for Ramsey-CPT microcell clocks [19].

The physical limitations to the short-term stability arise from the relatively high relaxation rates in the microcell that limit useful Ramsey times to $T_R \leq 400 \mu\text{s}$, with an optimum around $250 \mu\text{s}$. The dependence of stability on T_R is relatively flat and wide, and operating closer to its upper end gives an additional margin for the Dick effect contribution. Our short-term stability analysis shows that this may be particularly useful in view of future implementation of a miniaturized microwave source with relaxed phase noise specifications, while degrading the overall stability by less than a factor of 2.

In the present study, we use a frequency-stabilized laser head and AOM for generating the optical pulses. In future studies, a much smaller and low-power laser source like a VCSEL could be implemented in view of a miniaturized and low-power atomic clock. Furthermore, alternative optical switching means are of interest for replacing the AOM, for instance direct current modulation of a VCSEL as studied for CPT-based clocks [49,50].

The main advantage of the μ POP approach lies in the very low light-shift effects that are among the main limitations to the long-term stability in cw miniature atomic clocks. Further studies are of interest to address a complete long-term instability budget of the μ POP clock in view of fully exploiting its improved stability potential.

ACKNOWLEDGMENTS

This work has received funding from the European Union's Horizon 2020 research and innovation programme under Grant Agreement No. 820393, macQsimal project. We also acknowledge support from the European Space Agency (ESTEC Contracts No. 4000101390 and No. 4000129974/20/NL/LW) and from University of Neuchâtel. We thank P. Scherler and M. Durrenberger for technical support. The experimental data presented in this work is accessible open access under DOI: <https://b2share.eudat.eu/records/12c17379d9b443a693ec5a2e54abb8d7>.

- [1] S. Knappe, in *MEMS Atomic Clocks Comprehensive Microsystems*, edited by Y. B. Gianchandani, et al., Vol. 3.
- [2] R. Lutwak, A. Rashed, M. Varghesea, G. Tepolt, J. LeBlanc, M. Mescher, D. K. Serkland, K. M. Geib, G. M. Peake, and S. Römisch, in *39th Annual Precise Time and Time Interval (PTTI) Meeting* (2007).
- [3] S. Bregni, *Synchronization of Digital Telecommunications Networks* (John Wiley & Sons, Hoboken NJ, USA, 2002).
- [4] A. T. Gardner and J. A. Collins, in *2012 Oceans* (IEEE, 2012), pp. 1–8.
- [5] E. Fernández, D. Calero, and M. E. Parés, CSAC characterization and its impact on GNSS clock augmentation performance, *Sensors* **17**, 370 (2017).
- [6] L.-A. Liew, S. Knappe, J. Moreland, H. Robinson, L. Hollberg, and J. Kitching, Microfabricated alkali atom vapor cells, *Appl. Phys. Lett.* **84**, 2694 (2004).
- [7] E. Arimondo, in *Progress in Optics*, edited by E. Wolf (Elsevier, Amsterdam, 1996), Vol. 35, p. 257.
- [8] C. Affolderbach, A. Nagel, S. Knappe, C. Jung, D. Wiedenmann, and R. Wynands, Nonlinear spectroscopy with a vertical-cavity surface-emitting laser (VCSEL), *Appl. Phys. B Lasers Opt.* **70**, 407 (2000).
- [9] M. Abdel Hafiz, G. Coget, M. Petersen, C. E. Calosso, S. Guérandel, E. de Clercq, and R. Boudot, Symmetric autobalanced Ramsey interrogation for high-performance coherent-population-trapping vapor-cell atomic clock, *Appl. Phys. Lett.* **112**, 244102 (2018).
- [10] M. Abdel Hafiz, R. Vicarini, N. Passilly, C. E. Calosso, V. Maurice, J. W. Pollock, A. V. Taichenachev, V. I. Yudin, J. Kitching, and R. Boudot, Protocol for Light-Shift Compensation in a Continuous-Wave Microcell Atomic Clock, *Phys. Rev. Appl.* **14**, 034015 (2020).
- [11] N. F. Ramsey, Experiments with separated oscillatory fields and hydrogen masers, *Science* **248**, 1612 (1990).
- [12] V. I. Yudin, A. V. Taichenachev, M. Y. Basalaev, T. Zanon-Willette, J. W. Pollock, M. Shuker, E. A. Donley, and J. Kitching, Generalized Autobalanced Ramsey Spectroscopy of Clock Transitions, *Phys. Rev. Appl.* **9**, 54034 (2018).
- [13] O. Kozlova, J. Danet, S. Guérandel, and E. de Clercq, Limitations of long-term stability in a coherent population trapping Cs clock, *IEEE Trans. Instrum. Meas.* **63**, 1863 (2014).
- [14] Y. Yano, W. Gao, S. Goka, and M. Kajita, Theoretical and experimental investigation of the light shift in Ramsey coherent population trapping, *Phys. Rev. A* **90**, 13826 (2014).
- [15] P. Yun, F. Tricot, C. E. Calosso, S. Micalizio, B. François, R. Boudot, S. Guérandel, and E. de Clercq, High-Performance Coherent Population Trapping Clock with Polarization Modulation, *Phys. Rev. Appl.* **7**, 014018 (2017).
- [16] M. Abdel Hafiz, G. Coget, M. Petersen, C. Rocher, S. Guérandel, T. Zanon-Willette, E. de Clercq, and R. Boudot, Toward a High-Stability Coherent Population Trapping Cs Vapor-Cell Atomic Clock Using Autobalanced Ramsey Spectroscopy, *Phys. Rev. Appl.* **9**, 064002 (2018).
- [17] V. I. Yudin, M. Y. Basalaev, A. V. Taichenachev, J. W. Pollock, Z. L. Newman, M. Shuker, A. Hansen, M. T. Hummon, R. Boudot, E. A. Donley, *et al.*, General Methods for Suppressing the Light Shift in Atomic Clocks Using Power Modulation, *Phys. Rev. Appl.* **14**, 1 (2020).
- [18] E. Blanshan, S. M. Rochester, E. A. Donley, and J. Kitching, Light shifts in a pulsed cold-atom coherent-population-trapping clock, *Phys. Rev. A* **91**, 41401 (2015).
- [19] C. Carlé, M. Petersen, N. Passilly, M. A. Hafiz, E. De Clercq, and R. Boudot, Exploring the use of Ramsey-CPT spectroscopy for a microcell-based atomic clock, *IEEE Trans. Ultrason. Ferroelectr. Freq. Control* **68**, 3249 (2021).
- [20] J. Camparo, The rubidium atomic clock and basic research, *Phys. Today* **60**, 33 (2007).
- [21] N. Almat, M. Gharavipour, W. Moreno, C. Affolderbach, and G. Mileti, in *2019 Joint Conference of the IEEE International Frequency Control Symposium and European Frequency and Time Forum (EFTF/IFC)* (IEEE, 2019), Vol. 67, pp. 1–2.
- [22] S. Micalizio, F. Levi, C. E. Calosso, M. Gozzelino, and A. Godone, A pulsed-laser Rb atomic frequency standard for GNSS applications, *GPS Solut.* **25**, 94 (2021).
- [23] Q. Shen, H. Lin, J. Deng, and Y. Wang, Pulsed optically pumped atomic clock with a medium- to long-term frequency stability of 10^{-15} , *Rev. Sci. Instrum.* **91**, 045114 (2020).
- [24] Q. Hao, W. Xue, W. Li, F. Xu, X. Wang, W. Guo, P. Yun, and S. Zhang, Microwave pulse-coherent technique-based clock with a novel magnetron-type cavity, *IEEE Trans. Ultrason. Ferroelectr. Freq. Control* **67**, 873 (2020).
- [25] J. C. Camparo, R. P. Frueholz, and C. H. Volk, Inhomogeneous light shift in alkali-metal atoms, *Phys. Rev. A* **27**, 1914 (1983).
- [26] F. Levi, J. Camparo, B. Francois, C. E. Calosso, S. Micalizio, and A. Godone, Precision test of the ac Stark shift in a rubidium atomic vapor, *Phys. Rev. A* **93**, 23433 (2016).
- [27] M. Gharavipour, C. Affolderbach, S. Kang, T. Bandi, F. Gruet, M. Pellaton, and G. Mileti, High performance vapour-cell frequency standards, *J. Phys. Conf. Ser.* **723**, 12006 (2016).
- [28] M. Pellaton, C. Affolderbach, Y. Pétremand, N. de Rooij, and G. Mileti, Study of laser-pumped double-resonance clock signals using a microfabricated cell, *Phys. Scr.* **2012**, 14013 (2012).
- [29] M. Violetti, M. Pellaton, C. Affolderbach, F. Merli, J.-F. Zurcher, G. Mileti, and A. K. Skrivervik, The microloop-gap resonator: A novel miniaturized microwave cavity for double-resonance rubidium atomic clocks, *IEEE Sens. J.* **14**, 3193 (2014).
- [30] Y. Pétremand, C. Affolderbach, R. Straessle, M. Pellaton, D. Briand, G. Mileti, and N. F. de Rooij, Microfabricated rubidium vapour cell with a thick glass core for small-scale atomic clock applications, *J. Micromech. Microeng.* **22**, 25013 (2012).
- [31] C. B. Alcock, V. P. Itkin, and M. K. Horrigan, Vapor pressure equations for the metallic elements: 298–2500 K, *Can. Metall. Q.* **23**, 309 (1984).
- [32] T. Bandi, C. Affolderbach, C. Stefanucci, F. Merli, A. K. Skrivervik, and G. Mileti, Compact high-performance continuous-wave double-resonance rubidium standard with 1.4×10^{-13} Tau $^{-1/2}$ stability, *IEEE Trans. Ultrason. Ferroelectr. Freq. Control* **61**, 1769 (2014).

- [33] F. Gruet, M. Pellaton, C. Affolderbach, T. Bandi, R. Matthey, and G. Mileti, in *Proc. ICSSO* (2012).
- [34] S. Kang, M. Gharavipour, F. Gruet, C. Affolderbach, and G. Mileti, in *2015 Joint Conference of the IEEE International Frequency Control Symposium the European Frequency and Time Forum* (2015), pp. 800–803.
- [35] E. Batori, N. Almat, C. Affolderbach, F. Gruet, and G. Mileti, in *2020 European Navigation Conference (ENC)* (IEEE, 2020), pp. 1–10.
- [36] J. C. Camparo, Conversion of laser phase noise to amplitude noise in an optically thick vapor, *J. Opt. Soc. Am. B* **15**, 1177 (1998).
- [37] C. E. Calosso, S. Micalizio, A. Godone, E. K. Bertacco, and F. Levi, Electronics for the pulsed rubidium clock: Design and characterization, *IEEE Trans. Ultrason. Ferroelectr. Freq. Control* **54**, 1731 (2007).
- [38] S. Micalizio, C. E. Calosso, F. Levi, and A. Godone, Ramsey-fringe shape in an alkali-metal vapor cell with buffer gas, *Phys. Rev. A* **88**, 33401 (2013).
- [39] M. Gozzelino, S. Micalizio, C. E. Calosso, A. Godone, and F. Levi, Kr-Based buffer gas for rb vapor-cell clocks, *IEEE Trans. Ultrason. Ferroelectr. Freq. Control* **68**, 1442 (2021).
- [40] W. Franzen, Spin relaxation of optically aligned rubidium vapor, *Phys. Rev.* **115**, 850 (1959).
- [41] S. Micalizio, A. Godone, F. Levi, and C. Calosso, Pulsed optically pumped 87Rb vapor cell frequency standard: A multilevel approach, *Phys. Rev. A* **79**, 013403 (2009).
- [42] W. Moreno, Université de Neuchâtel., 2019.
- [43] M. Gharavipour, C. Affolderbach, F. Gruet, I. S. Radojčić, A. J. Krmpot, B. M. Jelenković, and G. Mileti, Optically-detected spin-echo method for relaxation times measurements in a Rb atomic vapor, *New J. Phys.* **19**, 063027 (2017).
- [44] V. Shah and J. Kitching, in *Advances in Atomic, Molecular and Optical Physics*, edited by E. Arimondo (Elsevier Inc, Amsterdam, 2010), Vol. 59, p. 21.
- [45] C. E. Calosso, M. Gozzelino, A. Godone, H. Lin, F. Levi, and S. Micalizio, Intensity detection noise in pulsed vapor-cell frequency standards, *IEEE Trans. Ultrason. Ferroelectr. Freq. Control* **67**, 1074 (2020).
- [46] S. Micalizio, C. E. Calosso, A. Godone, and F. Levi, Metrological characterization of the pulsed Rb clock with optical detection, *Metrologia* **49**, 425 (2012).
- [47] T4Science, PHMaser 1008 Passive Hydrogen Maser Clock.
- [48] Z. L. Newman, V. Maurice, T. Drake, J. R. Stone, T. C. Briles, D. T. Spencer, C. Fredrick, Q. Li, D. Westly, B. R. Ilic, *et al.*, Architecture for the photonic integration of an optical atomic clock, *Optica* **6**, 680 (2019).
- [49] Y. Yano, S. Goka, and M. Kajita, Two-step pulse observation to improve resonance contrast for coherent population trapping atomic clock, *Appl. Phys. B Lasers Opt.* **123** (2017).
- [50] T. Ide, S. Goka, and Y. Yano, in *2015 Jt. Conf. IEEE Int. Freq. Control Symp. Eur. Freq. Time Forum, FCS 2015 - Proc.* (2015), Vol. 978, p. 167.